

# Thermoacoustic heat pump utilizing medium/low-grade heat sources for domestic building heating

Yiwei Hu<sup>a,b</sup>, Kaiqi Luo<sup>c</sup>, Dan Zhao<sup>d</sup>, Zhanghua Wu<sup>a</sup>, Yupeng Yang<sup>a,b</sup>, Ercang Luo<sup>a,b</sup>, Jingyuan Xu<sup>e,\*</sup>

<sup>a</sup> Chinese Academy of Science, Key Laboratory of Cryogenics, Technical Institute of Physics and Chemistry, Beijing 100190, China

<sup>b</sup> University of Chinese Academy Science, Beijing 100049, China

<sup>c</sup> Building Energy Research Center, Tsinghua University, Beijing 100084, China

<sup>d</sup> Department of Mechanical Engineering, Faculty of Engineering, University of Canterbury, Private Bag 4800, Christchurch 8041, New Zealand

<sup>e</sup> Institute of Microstructure Technology, Karlsruhe Institute of Technology, Karlsruhe 76344, Germany

## ARTICLE INFO

### Keywords:

Thermoacoustic heat pump  
Thermodynamics  
Heat pump  
Medium/low-grade heat  
Domestic heating

## ABSTRACT

Thermoacoustic heat pumps are a promising heating technology that utilizes medium/low-grade heat to reduce reliance on electricity. This study proposes a single direct-coupled configuration for a thermoacoustic heat pump, aimed at minimizing system complexity and making it suitable for domestic applications. Numerical investigations were conducted under typical household heating conditions, including performance analysis, exergy loss evaluation, and axial distribution of key parameters. Results show that the proposed thermoacoustic heat pump achieves a heating capacity of 5.7 kW and a coefficient of performance of 1.4, with a heating temperature of 300 °C and a heat-sink temperature of 55 °C. A comparison with existing absorption heat pumps reveals favorable adaptability for large temperature lift applications. A case study conducted in Finland over an annual cycle analyzes the economic and environmental performance of the system, identifying two distinct modes based on the driving heat source: medium temperature ( $\geq 250$  °C) and low temperature ( $< 250$  °C), both of which exhibit favorable heating performance. When the thermoacoustic heat pump is driven by waste heat, energy savings of 20.1 MWh/year, emission reductions of 4143 kgCO<sub>2</sub>/year, and total environmental cost savings of 1629 €/year are obtained. These results demonstrate the potential of the proposed thermoacoustic heat pump as a cost-effective and environmentally friendly option for domestic building heating using medium/low-grade heat sources.

## 1. Introduction

Heating constitutes a significant portion of energy consumption in society. Residential dwellings account for 28% of the final energy consumption in the EU in 2020, second only to the transport sector (28.4%) [1]. Of this share, about 80% of the energy was dedicated to space heating and hot water supply [2]. 300 TWh/year of the total waste heat potential is reported in the EU, with about 60% corresponding to the temperature range of 200–500 °C, which is often referred to as medium/low-temperature waste heat [3]. The rational recovery of waste heat has the potential to improve energy efficiency by 10–50% [4]. Although heat pumps based on vapor compression technology are commonly used for domestic heating due to their high efficiency [5], there is a pressing need for a technological transformation towards zero carbon solutions to achieve the goal of net-zero carbon emissions by 2050

[6]. Additionally, the over-reliance on electricity for heat pumps can lead to challenges such as high loads on the transmission network [7].

The utilization of heat-driven thermoacoustic heat pump (TAHP) systems has emerged as a promising solution for household heating applications, given the several benefits that it offers. TAHPs are capable of operating solely on medium/low-grade heat sources, including solar, geothermal, and waste heat, thereby decreasing the dependence on electricity. This feature is particularly advantageous for remote areas where electricity is not readily available. Additionally, TAHP systems are characterized by their versatility in heat source utilization and high energy efficiency [8]. Furthermore, TAHPs make use of environmentally friendly working gases, such as helium and nitrogen, and have an extended life expectancy since they do not contain mechanical moving parts [9]. These advantages make TAHPs a viable and cost-effective solution for household heating applications, especially in regions where

\* Corresponding author.

E-mail addresses: [ec Luo@mail.ipc.ac.cn](mailto:ec Luo@mail.ipc.ac.cn) (E. Luo), [jingyuan.xu@kit.edu](mailto:jingyuan.xu@kit.edu) (J. Xu).

<https://doi.org/10.1016/j.enbenv.2023.06.006>

Received 15 April 2023; Received in revised form 30 May 2023; Accepted 15 June 2023

Available online xxx

2666-1233/Copyright © 2023 Southwest Jiatong University. Publishing services by Elsevier B.V. on behalf of KeAi Communication Co. Ltd. This is an open access article under the CC BY-NC-ND license (<http://creativecommons.org/licenses/by-nc-nd/4.0/>)

## Nomenclatures

### Symbols

A	area, m <sup>2</sup>
c <sub>p</sub>	specific heat capacity, J/(kg·K)
D	diameter, m
d <sub>h</sub>	hydraulic diameter, m
e	mass-specific total gas energy, J/kg
f	frequency, Hz
f <sub>D</sub>	Darcy friction factor
F	viscous pressure gradient
k	thermal conductivity, W/(m·K)
l	length, m
p	pressure, Pa
Pr	Prandtl number
q	instantaneous axial heat flux, W/m <sup>2</sup>
Q <sub>w</sub>	film heat transfer, W
Q	rate at which heat is transferred, W
T	temperature, K
U	volume flow rate, m <sup>3</sup> /s
V	volume, m <sup>3</sup>
W <sub>a</sub>	acoustic power, W
η	thermoacoustic efficiency
ρ	density, kg/m <sup>3</sup>
μ	dynamic viscosity, kg/(m·s)
μ <sub>g,0</sub>	gas dynamic viscosity, kg/(m·s)
Φ	porosity
θ	phase angle, °
	determinant of the matrix

### Abbreviations

AHX	ambient-temperature heat exchanger
COP	coefficient of performance
C <sub>s</sub>	cost saving
EPCS	environment penalty cost saving
ER	CO <sub>2</sub> emission reduction
FES	fuel energy saving
HX	heat exchanger
HHX	heating heat exchanger
HSHX	heat-source heat exchanger
PT	pulse tube
REG	regenerator
SHX	heat-sink heat exchanger
TBT	thermal buffer tube
TCS	total cost saving
TAHP	thermoacoustic heat pump

### Subscripts

a	ambient
dem	demand
e	engine
g	gas
h	heating/heat pump/hour
in	input
m	mean/month
out	output
sub	subunit
κ	thermal
v	viscous
y	year

there is an abundance of medium/low-grade heat sources. Although it is challenging to accurately estimate the market potential for thermoacoustic heat pumps due to their current lack of mass production, their simple construction almost dictates that their market costs will be opti-

mistic. It is essential to continue exploring and improving TAHP systems' performance to maximize their benefits while minimizing their limitations.

Thermoacoustic heat pumps have received limited research attention so far, with most studies focused on refrigeration and power generation. The experimental research is still at the stage of laboratory prototypes. In 2004, Haywood et al. developed a thermoacoustic-Stirling type heat pump, which achieved a heating capacity of 2.2 kW at a heating temperature of 20 °C [10]. Similarly, Mohamed et al. demonstrated a thermoacoustic heat pump functioning as a heater in 2011, which generated a heating temperature of 370 °C [11]. In 2015, Yang et al. constructed a linear-compressor-driven travelling-wave thermoacoustic heat pump for ultra-low temperature operation and achieved a heating capacity of 260 W at an ambient temperature of -20 °C [12]. More recently, Li et al. built a 1 kW-class thermoacoustic-Stirling type heat pump and achieved a maximum coefficient of performance for heating (COP<sub>h</sub>) of 1.4 under heating and ambient temperatures of 50 °C and -20 °C, respectively [13]. Widyaparaga et al. reported a maximum temperature difference of 23 °C in a dual-acoustic driven thermoacoustic heat pump in 2020 [14]. Additionally, in 2022, Yang et al. proposed a two-stage looped heat-driven thermoacoustic system for combined cooling and heating and achieved a maximum COP<sub>h</sub> of 1.24 when operating as a heat pump [8].

In recent years, theoretical investigations have also been carried out to enhance the understanding of thermoacoustic heat pumps. In 2014, Mohammad et al. employed a multi-objective optimization approach to study irreversible Stirling heat pump cycles, with the objective of maximizing the heating load and coefficient of performance while minimizing the input power of the heat pump simultaneously [15]. Subsequently, they proposed a thermo-economic optimization method utilizing a non-dominated sorting genetic algorithm [16]. In 2014, Barreno et al. put forth a preliminary design of a thermoacoustic-Stirling type heat pump and analyzed the stability of its operation by considering possible variations in working conditions [17]. In 2019, Sun et al. proposed a gas-fired heat-driven thermoacoustic heat pump system that achieved a COP<sub>h</sub> of 1.72 with a heating temperature of 60 °C and an ambient temperature of 0 °C [18]. In 2020, Khan et al. conducted an assessment of a 500 kW-class thermoacoustic-Stirling type heat pump in terms of its environmental footprint over a 15-year period [19]. Comparative results with natural gas-fired and oil-fired boilers demonstrated that the thermoacoustic-Stirling type heat pump could reduce environmental impact by at least 10% up to over 40%. Cheng et al. simulated a beta-type Stirling heat pump using a thermodynamic model, obtaining a heating power of 904 W for hot water at 38 °C [20]. In 2021, Xu et al. simulated a thermoacoustic combined cooling, heating, and power (CCHP) system that obtained a heating power of 3.55 kW with an overall exergy efficiency of 24.1% [21]. In 2022, Yang et al. presented a theoretical study on a phase-change travelling-wave TAHP system, demonstrating the potential for efficient and cost-effective heat pumping [22]. Similarly, in the same year, Chen et al. simulated a dual-acoustic driver TAHP system, confirming the significance of establishing a traveling-wave acoustic field for generating larger temperature differences [23].

Currently, available thermoacoustic devices driven by thermoacoustic engines have multiple core units [24–26], and the phase shifter regulates the acoustic fields to meet the requirement of a 360°/N phase angle difference between the entrance and exit of the thermoacoustic core unit, where N is the number of core units. However, the complexity of integrating these multi-unit thermoacoustic heat pumps with existing household heating and cooling water systems poses a significant challenge, limiting their practical application for household heating. Additionally, inconsistent working conditions among individual units further impede long-term and stable operations [27]. As a result, recent research efforts have shifted towards the development of single-unit thermoacoustic heat pump (TAHP) systems. This necessitates the design of a new phase shifter capable of achieving a 360° phase angle difference between the exit and entrance of the thermoacoustic unit since conventional resonant tubes fail to meet this requirement. Furthermore, while previous

studies have proposed multi-core unit thermoacoustic devices for operation in the room temperature zone, these ideas remain conceptual [28]. In practical applications, the heat load varies, and although some previous studies have provided system performance under different operating conditions to some extent [8], they fall short of meeting the actual demand. Therefore, this research aims to bridge these gaps through a comprehensive analysis of energy, environmental, and economic indicators of a thermoacoustic heat pump system. The study introduces novel elements that contribute to the expanding body of knowledge in this field:

- To the best of the authors' knowledge, there are currently no reported simulations or experiments concerning single-unit direct-coupling thermoacoustic heat pump systems. This research presents a novel system that incorporates a cavity structure at an optimal location and investigates its thermodynamic and thermoacoustic characteristics. The adoption of this approach offers several advantages, including the minimization of system complexity and the resolution of performance instability issues.
- To date, there have been no reported investigations that combine thermoacoustic heat pumps with practical applications. In light of this gap, this study examines the practical application potential of the proposed system by conducting a case study focused on a typical household in Finland. By doing so, the research aims to provide insights into the real-world implementation of thermoacoustic heat

pumps and their feasibility for residential heating applications in specific geographical contexts.

- The existing body of work on thermoacoustic heat pump systems primarily focuses on thermodynamic and thermoacoustic performance analyses. In contrast, this research expands the scope by conducting a comprehensive assessment of the proposed system's combined energetic performance, economic viability, and environmental potential. This study incorporates quantitative analysis to evaluate the energy-saving benefits and environmental impact of employing thermoacoustic heat pump systems for household heating applications.
- In the present research, the heating performance of the thermoacoustic heat pump is further compared to more conventional absorption heat pumps at different temperature lifts, for the first time.

## 2. System description

Fig. 1 (a) shows the schematic of a heat-driven thermoacoustic heat pump (TAHP) system, which comprises a single direct-coupling energy-conversion core unit and a phase-shifter unit. The core unit consists of an engine stage and a heat pump stage. The engine stage includes a heat-sink heat exchanger (SHX<sub>e</sub>), a regenerator (REG<sub>e</sub>), a heating heat exchanger (HHX<sub>e</sub>), and a thermal buffer tube (TBT<sub>e</sub>). The heat pump stage consists of a cooler, which includes a heat-sink temperature heat exchanger (SHX<sub>h</sub>), a regenerator (REG<sub>h</sub>), a heat-source heat exchanger (HSHX<sub>h</sub>), and a thermal buffer tube (TBT<sub>h</sub>). The phase-shifter unit com-

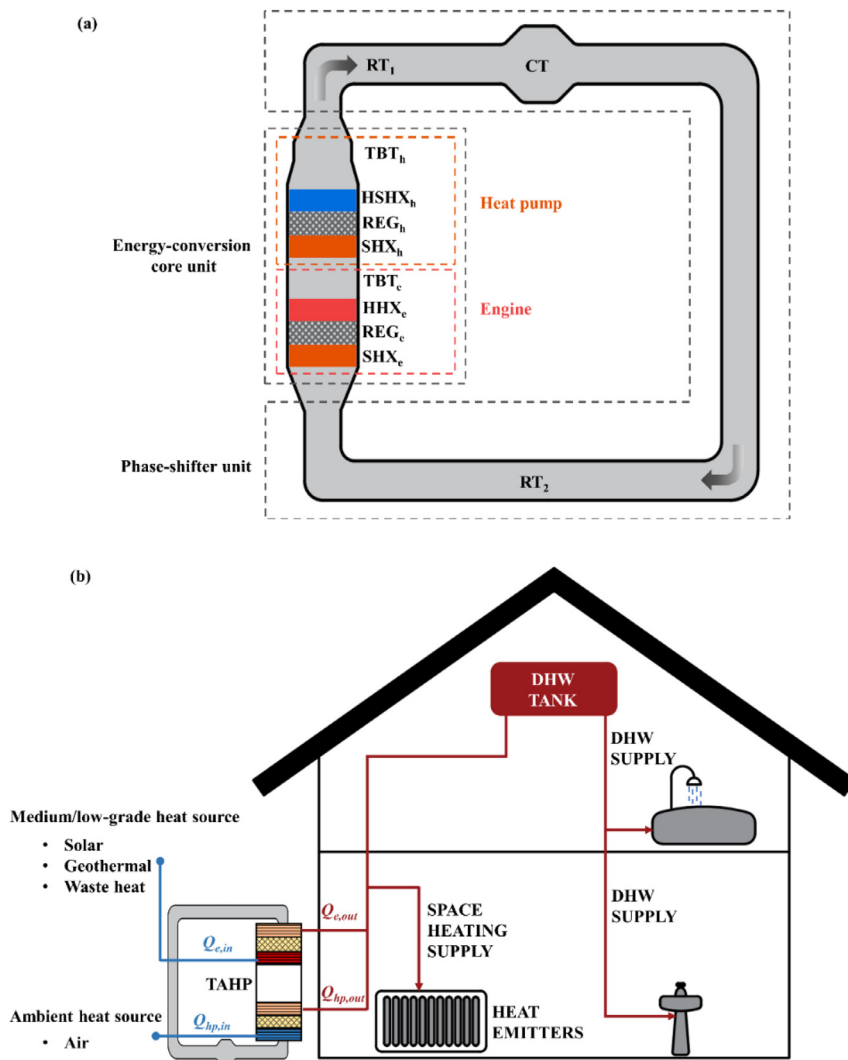


Fig. 1. (a) Schematic of a heat-driven thermoacoustic heat pump (TAHP) system with a single direct-coupling configuration. (b) Envisioned configuration of a heat-driven thermoacoustic heat pump (TAHP) system for domestic applications including space heating and hot-water supply. SHX is the heat-sink heat exchanger, REG is the regenerator, HHX is the heating heat exchangers, TBT is the thermal buffer tube, HSHX is the heat-source heat exchanger, RT is the resonant tube, CT is the cavity, and  $Q$  is the heat flow.  $e$  is for the engine and  $h$  is for the heat pump. The subscript  $in$  means input and  $out$  means output.

**Table 1**  
Dimensions of each component of the TAHP system.

Subunit	Parts	Diameter (mm)	Length (mm)	Other dimensions
Engine	SHX <sub>e</sub>	150	33	Shell tube type, 11% in porosity, 1 mm in internal diameter
	REG <sub>e</sub>	150	40	76% in porosity, 50 μm in wire diameter
	HHX <sub>e</sub>	150	33	Shell tube type, 11% in porosity, 1 mm in internal diameter
	TBT <sub>e</sub>	150	100	7 mm in wall thickness
Heat pump	SHX <sub>h</sub>	150	33	Shell tube type, 11% in porosity, 1 mm in internal diameter
	REG <sub>h</sub>	150	35	73% in porosity, 50 μm in wire diameter
	HSHX <sub>h</sub>	150	33	Shell tube type, 11% in porosity, 1 mm in internal diameter
	TBT <sub>h</sub>	90	50	7 mm in wall thickness
Phase shifter	RT <sub>1</sub>	54	2150	1E-3 in relative roughness
	CT	115	500	1 mm in wall thickness
	RT <sub>2</sub>	54	9650	1E-3 in relative roughness

prises two resonators (RT<sub>1</sub> and RT<sub>2</sub>) and a cavity (CT), and it is used to regulate the phase relationship between the pressure and volume flow rate at the inlet and outlet of the core unit, in order to achieve suitable acoustic matching.

Fig. 1 (b) illustrates the envisioned configuration of a heat-driven thermoacoustic heat pump (TAHP) system for domestic applications, including space heating and domestic hot water (DHW) supply. The system operates as follows: self-excited thermoacoustic oscillation is initiated when the axial temperature gradient across the regenerator (REG<sub>e</sub>) reaches a critical value, leading to the conversion of heat to acoustic power. The amplified acoustic power is then utilized to drive the heat pump stage, which transfers heat from the heat source to the heat sink. The heating heat exchanger (HHX<sub>e</sub>) is heated by the medium/low-grade heat source (e.g., solar, geothermal, waste heat), while the heat-source heat exchanger (HSHX<sub>h</sub>) is cooled by the ambient heat source (e.g., air). The heat-sink heat exchangers (SHX<sub>s</sub>) are maintained at the desired indoor heating temperature by circulating water to be heated. Table 1 provides the geometric dimensions of the main components of the TAHP system.

### 3. Model description and validation

The numerical simulations of the heat-driven thermoacoustic heat pump (TAHP) system are conducted using the Sage program [29], which is a widely used software for modeling and calculating thermoacoustic devices [30–34]. The Sage program is based on a time-domain model, and it solves the conservation equations of mass, momentum, and energy in the gas domain. These equations are used to describe the thermodynamic and acoustic behavior of the TAHP system during operation:

$$\frac{\partial \rho A}{\partial t} + \frac{\partial \rho u A}{\partial x} = 0 \quad (1)$$

$$\frac{\partial \rho u A}{\partial t} + \frac{\partial u \rho u A}{\partial x} + \frac{\partial p}{\partial x} A - F A = 0 \quad (2)$$

$$\frac{\partial \rho e A}{\partial t} + p \frac{\partial A}{\partial t} + \frac{\partial}{\partial x} (u \rho e A + u p A + q) - Q_w = 0 \quad (3)$$

where  $\rho$  is the density of the working medium,  $A$  denotes the cross-sectional area of the channel, and  $u$  is the velocity in the  $x$ -direction.  $F$ ,  $q$ , and  $Q_w$  are the viscous pressure gradient, the heat flux by axial conduction of gases, and the heat flow per unit length through the negative  $z$  surface caused by film heat transfer, respectively.  $e = \kappa + u^2/2$  is the mass-specific total gas energy and  $\kappa$  is the mass-specific internal gas energy.  $p$  denotes the pressure.

According to the empirical functions, the terms  $F$ ,  $q$  and  $Q_w$  can be expressed as,

$$F = -(f_D/d_h + K_{los}/l)\rho u|u|/2 \quad (4)$$

$$q = -N_k k_g \frac{\partial T}{\partial x} A \quad (5)$$

$$Q_w = Nu(k_g/d_h)S_x(T_w - T) \quad (6)$$

where  $f_D$ ,  $d_h$ , and  $K_{los}$  are the Darcy friction factor, hydraulic diameter, and the total local loss coefficient, respectively.  $N_k$  is an axial conductivity enhancement ratio that is represented as a ratio of the effective gas conductivity to the molecular conductivity.  $k_g$  is the gas conductivity.  $Nu$ ,  $S_x$ , and  $(T_w - T)$  denote the Nusselt number, the wetted perimeter, and the temperature difference between the negative  $z$  surface and the section average, respectively.

To characterize the thermoacoustic heat pump, some parameters are employed as shown in Appendix. A.

To validate the simulation, an experimental prototype of a two-stage thermoacoustic heat pump system was built. The experimental setup is shown in Fig. 2 (a) and (b), and the system consists of two similar thermoacoustic core units. Fig. 3 (a) and (b) compare the numerical and experimental results of the output heating capacity ( $Q_{out}$ ) and coefficient of performance (COP) under different heat-source temperatures respectively. The average deviations on  $Q_{out}$  and COP are 3.5% and 3.6%, respectively. This verification indicates that the presented TAHP system can be satisfactorily simulated by the Sage program, demonstrating the accuracy and reliability of the numerical simulations.

## 4. Results and discussion

### 4.1. System performance and exergy loss analysis

Table 2 lists the simulation results of the proposed TAHP system at the nominal condition for household heating applications. The heat-sink temperature ( $T_{sink}$ ) is set at 55 °C, which is reported as the minimum temperature to prevent harmful bacteria in the hot water supply [35]. The heat-source temperature ( $T_{source}$ ) is set at 7 °C, following the industrial standard in the heat pump field [36]. The heating temperature of the HHX<sub>e</sub> ( $T_h$ ) is set at 300 °C, as the intention is to utilize medium/low-grade temperature heat. Under these working conditions, the TAHP system is shown to provide an output heating capacity ( $Q_{out}$ ) of 5.7 kW, a coefficient of performance (COP) of 1.4, and a relative Carnot efficiency ( $\eta$ ) of 39.9%.

**Table 2**

Numerical results of the TAHP system for the specific working condition.

Symbol	Parameter	Value
$P_m$	Mean pressure (MPa)	10
$P_r$	Pressure ratio at inlet of engine stage	1.07
$T_h$	Heating temperature of the engine stage (K)	573
$T_{source}$	Temperature of the heat source (K)	280
$T_{sink}$	Temperature of the heat sink (K)	328
$f$	Working frequency (Hz)	72.2
$Q_{e,in}$	Input heating power in engine stage (kW)	4.1
$Q_{out}$	Output heating capacity of the system (kW)	5.7
COP	Coefficient of performance of the system	1.4
$\eta$	Relative Carnot efficiency of the system	39.9%

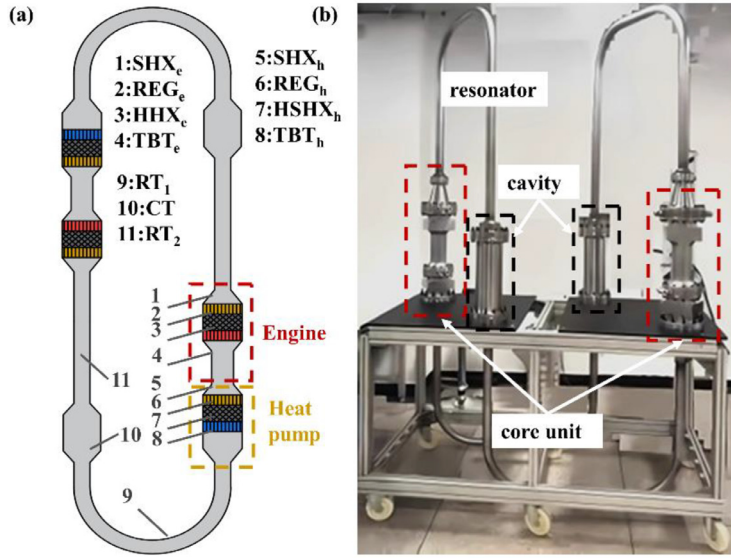


Fig. 2. Experimental setup of the two-stage thermoacoustic heat pump system: (a) schematic of the system and (b) prototype photograph of the system.

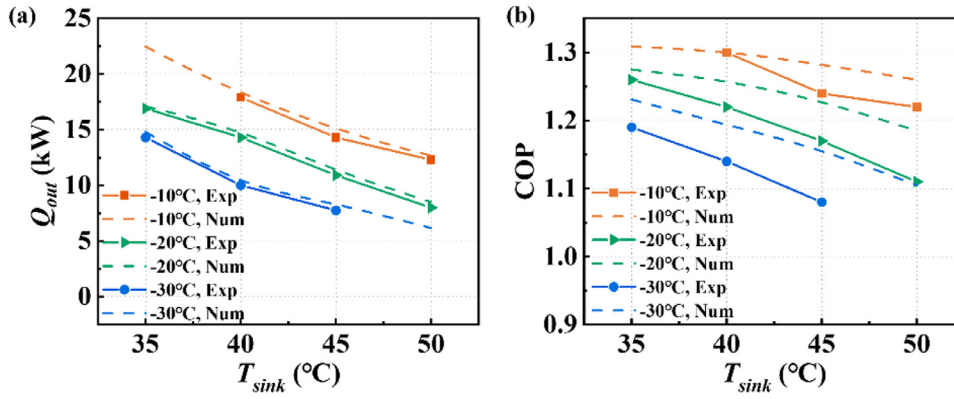


Fig. 3. Comparison of numerical and experimental results of the two-stage thermoacoustic heat pump under different heat-source temperatures ( $T_h=573$  K,  $P_m=10$  MPa): (a) Output heating capacity ( $Q_{out}$ ), (b) coefficient of performance (COP) of the system.  $T_h$ ,  $T_{sink}$ , and  $P_m$  denote the heating temperature, heat-sink temperature, and mean pressure.

Exergy loss distribution analysis is conducted to assess the system's structural parameters and identify areas for further improvements. The typical sources of exergy loss in the system include flow friction loss ( $AE_{fric}$ ), non-ideal heat transfer loss ( $AE_{Qw}$ ) between the gas and the solid, and axial heat flow loss ( $AE_{Qx}$ ). These losses can be expressed as:

$$AE_{fric} = -T_0 \times \oint \frac{uAF}{T} \quad (7)$$

$$AE_{Qw} = -T_0 \times \oint \frac{q_w \cdot \nabla T_w}{T^2} \quad (8)$$

$$AE_{Qx} = -T_0 \times \oint \frac{q_x \cdot \nabla T_x}{T^2} \quad (9)$$

where  $q$  and  $\nabla T$  respectively represent the heat flux and the temperature gradient. The subscript  $x$  means the term between gas and solid, and the subscript  $w$  means the term between gas and gas or between solid and solid.

According to the results of the exergy loss ratio in the main components of the TAHP system, as shown in Fig. 4, it is observed that the majority of the exergy loss occurs in the  $REG_e$ , accounting for 33.7% of the total exergy loss. This is attributed to the loud impedance in the regenerator, manifested as a significant proportion of non-ideal heat transfer losses and axial heat flow losses. Similar observations are made for the  $REG_h$ , which accounts for 20.2% of the total exergy loss. In the resonant tubes ( $RT_1$  and  $RT_2$ ), flow friction loss due to the large tube length

is the main contributor to the exergy loss, with 8.25% and 14.4% of exergy loss occurring in  $RT_1$  and  $RT_2$ , respectively. Other components in the system also exhibit varying degrees of exergy loss, primarily due to heat flow loss. These findings provide insights into the areas with

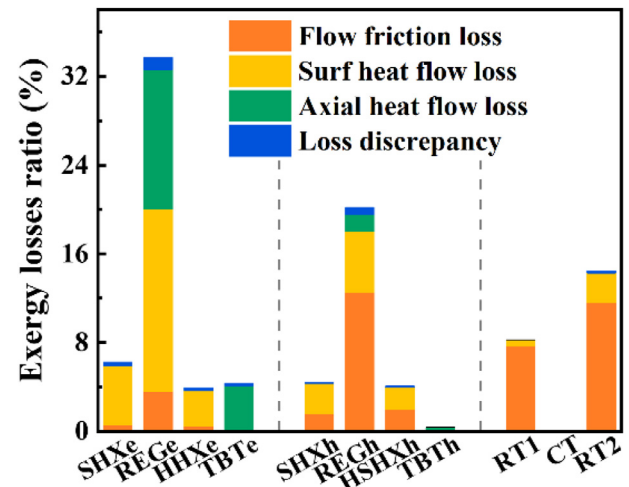


Fig. 4. Exergy loss analysis of each component. SHX is the heat-sink heat exchanger, REG is the regenerator, HHX is the heating heat exchangers, TBT is the thermal buffer tube, HSHX is the heat-source heat exchanger, RT is the resonant tube, and CT is the cavity.  $e$  is for the engine, and  $h$  is for the heat pump.

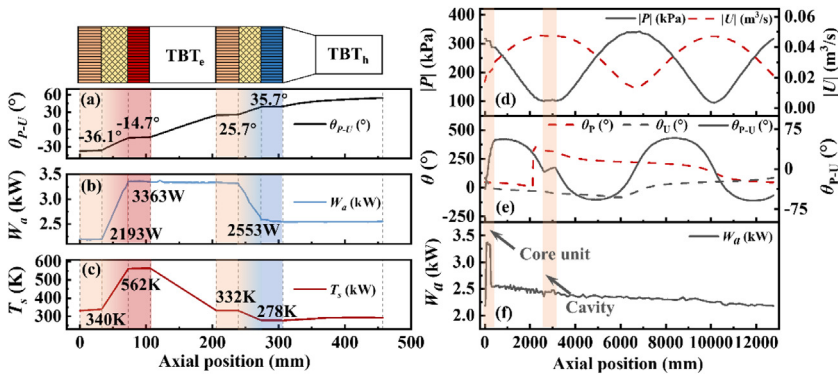


Fig. 5. Axial distributions of key parameters including the amplitude ( $|P|$ ) and phase ( $\theta_p$ ) of the pressure wave, the amplitude ( $|U|$ ) and phase ( $\theta_U$ ) of the volume flow rate, the phase difference between the two ( $\theta_{p,U}$ ), the gas temperature ( $T_s$ ), and the acoustic power ( $W_a$ ) of the system. (a-c) is for the core unit, and (d-f) is for the entire system.

higher exergy losses and offer guidance for potential improvements in the system's structural parameters to enhance overall performance.

#### 4.2. Axial distributions of key design parameters

Although conventional standing-wave thermoacoustic devices remain a subject of active research [37,38], the implementation of traveling-wave acoustic fields across the regenerators has been demonstrated to facilitate efficient energy conversion in thermoacoustic systems [39]. Hence, it is imperative to evaluate the thermoacoustic characteristics of the proposed TAHP system by examining the axial distributions of key parameters. The reference point for axial positioning is set at the inlet of SHX<sub>e</sub>. Regarding the core unit, Fig. 5 (a-c) illustrate the variation of the acoustic power ( $W_a$ ), the phase difference between the pressure wave and volume flow rate ( $\theta_{p,U}$ ), and the gas temperature ( $T_s$ ). The phase difference between the pressure wave and volume flow rate rises from  $-36.1^\circ$  to  $-14.7^\circ$  in the REG<sub>e</sub> and rises from  $25.7^\circ$  to  $35.7^\circ$  in the REG<sub>h</sub>, showing reasonable traveling-wave components. As for the acoustic power distributions, the original generation of approximately 2.2 kW of acoustic power is amplified to 3.4 kW in the engine stage and subsequently reduced to 2.6 kW after the utilization of the heat pump stage. For the entire system, Fig. 5 (d-f) shows the amplitude ( $|P|$ ) and phase ( $\theta_p$ ) of the pressure wave, the amplitude ( $|U|$ ) and phase ( $\theta_U$ ) of the volume flow rate, the phase difference between the two ( $\theta_{p,U}$ ), and the acoustic power ( $W_a$ ). Both  $|U|$  and  $|P|$  exhibit sinusoidal changes along the axial position, with careful consideration given to the peak value of pressure wave amplitude for stress verification in engineering. Furthermore, the phase angle distribution highlights the significant role played by the cavity structure in phase modulation and also reveals varying degrees of acoustic power loss in the core and phase shifter unit.

#### 4.3. Effect of the heating temperatures under different mean pressures

The heating temperature is dependent on the grade of the driven heat source. To investigate the potential of the proposed TAHP system in household heating applications, it is crucial to analyze the system's performance under varying heating temperatures. Fig. 6 shows the performance variation of the TAHP system with heating temperatures ranging from 525 K to 650 K, and mean pressures from 4 MPa to 10 MPa. Generally, an increase in heating temperature and mean pressure leads to improved input and output heat, but the impact on efficiency is not significant. However, when the mean pressure and heating temperature reach a certain level, there may be a slight decrease in efficiency due to increasing losses. Simultaneously, both parameters cannot be too small, as it may result in a significant reduction in system performance or even failure to initiate thermoacoustic oscillation. The optimum operating condition for performance is observed at a mean pressure of 6 MPa and

a heating temperature of 600 K, resulting in an output heating capacity of 3.9 kW and a COP of 1.4 for the TAHP system.

#### 4.4. Effect of the heat-sink and heat-source temperatures

The operating conditions of domestic heat pumps are determined by environmental factors, including heat-sink and heat-source temperatures, which significantly impact the heating performance of thermoacoustic heat pumps. Fig. 7 (a-d) illustrates the effect of heat-sink temperature on the heating performance under different heat-source temperatures. The heat-source temperature varies between 260 K and 310 K, representing the seasonal variations in air temperature. The heat-sink temperature ranges from 298 K to 363 K, encompassing the applications for low-temperature underfloor space heating to domestic hot water provision.

Generally, the input heating power, output heating capacity, and COP increase as the temperature difference between the heat sink and heat source decrease, while the efficiency ( $\eta$ ) exhibits the opposite trend. However, an exception is observed at heat-source temperatures of 260 K, 270 K, and 280 K, indicating the existence of an optimal heat-sink temperature for the relative Carnot efficiency of the system. The results demonstrate that the TAHP system can provide a stable output heating capacity with a COP ranging from 0.91 to 1.51 across the considered temperature range, indicating a promising potential for domestic heating applications in a wide temperature range. Specifically, in the typical domestic heating supply temperature range of  $50^\circ\text{C}$  to  $70^\circ\text{C}$ , the TAHP system can deliver an output heating capacity of 3 kW to 7 kW with a COP of 1.28 to 1.42 when the heat-source temperature is set at  $7^\circ\text{C}$ . Notably, the system performance at a heat-source temperature of 260 K and 270 K demonstrates that the TAHP system still works properly when the heat-source temperature is below  $0^\circ\text{C}$  and will not suffer from problems such as frosting, due to the using cryogenic working gases such as helium and nitrogen.

#### 4.5. Comparison with absorption heat pumps under different temperature lift

The thermoacoustic-Stirling type heat pump system has been reported to exhibit adaptability to different working temperatures and promising performance under high-temperature lift ( $\Delta T = T_h - T_{\text{source}}$ ) [11,40]. The performance of the proposed thermoacoustic heat pump system is studied in this section under different temperature lifts ( $\Delta T$ ) and compared with absorption heat pump (AHP) systems. The heating temperature of the TAHP system is set at  $350^\circ\text{C}$ , and the temperature lift between the heat-source and heat-sink temperature ( $\Delta T$ ) is varied from  $20^\circ\text{C}$  to  $90^\circ\text{C}$ . The results, as shown in Fig. 8, indicate that the coefficient of performance (COP) of the TAHP system decreases with an increase in temperature lift.

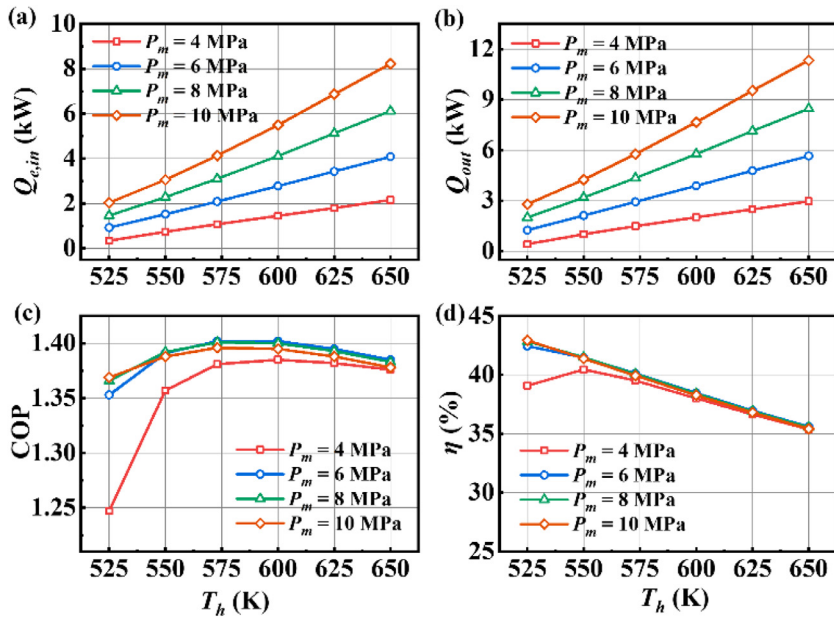


Fig. 6. Effect of the heating temperatures and mean pressures on system performance: (a) input heating power ( $Q_{e,in}$ ), (b) output heating capacity ( $Q_{out}$ ), (c) coefficient of performance (COP), (d) relative Carnot efficiency ( $\eta$ ) of the TAHP system.

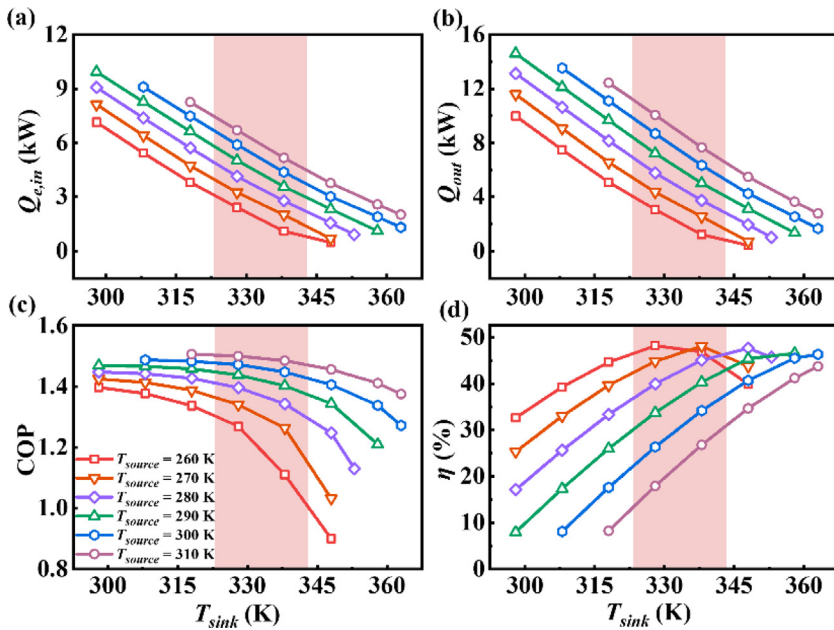


Fig. 7. Effect of the heat-sink and heat-source temperatures on system performance: (a) input heating power, (b) output heating capacity, (c) coefficient of performance, (d) relative Carnot efficiency of the TAHP system. The highlighted area in red relates to the typical domestic heating supply temperature range of 50 °C to 70 °C.

The comparison of COPs among different heat pump systems reveals that the double-effect AHP system exhibits the highest COP, followed by the single-effect AHP system. The TAHP system and the double-stage AHP system have comparable COPs. However, the TAHP system shows stable heating performance over a wide range of temperature lifts and promising performance in large temperature lift applications that AHP technology cannot achieve ( $\Delta T > 60$  °C). In contrast, the double-stage AHP system achieves a maximum temperature lift of about 60 °C, the single-effect about 50 °C, and the double-effect less than 25 °C. These findings suggest that the TAHP system has favorable potential for applications that require large temperature lifts, making it a promising option for high-temperature heat pump applications where AHP systems may not be as effective. Further studies and analysis of the energy, environmental, and economic indicators would provide a comprehensive evaluation of the performance and feasibility of the TAHP system in practical applications, especially in the context of domestic heating.

### 5. Economic and environmental analyses

In this section, a neural network model is proposed to assess the economic and environmental potential of the TAHP system, while reducing computational costs. Fig. 9 illustrates the flow chart of economic and environmental analyses combined with the neural network model. Firstly, the TAHP system's performance is evaluated at various specific operating conditions, including heating and heat-source temperatures. The results are utilized to generate a matrix of input variables and output performance, which is then iteratively trained until achieving the desired level of precision, as indicated by the coefficient of determination of the neural network model approaching 1. This signifies the successful learning of the relationship between input variables and output performance [44]. Subsequently, the annual hourly heating temperature and coefficient of performance variation of the TAHP system are obtained by substituting the hourly air temperature and heat demand values, re-

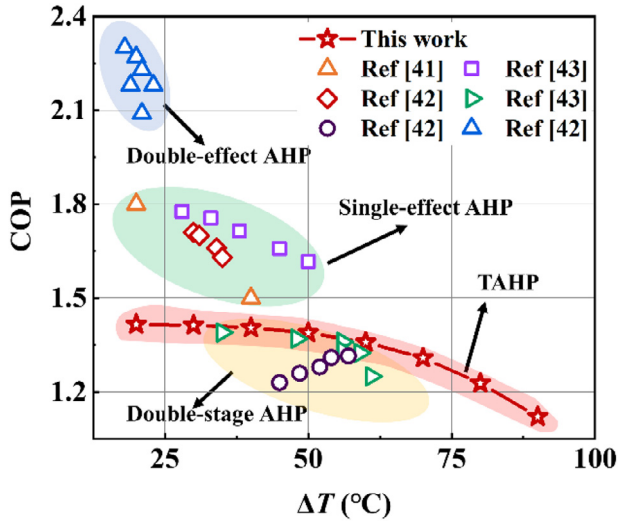


Fig. 8. Comparison of the TAHP and absorption heat pump (AHP) systems under different temperature lifts ( $\Delta T = T_{sink} - T_{source}$ ). The single-effect AHP [41–43], double-stage AHP [42,43], double-effect AHP [42], and TAHP are marked in blue, green and red, respectively.

trieved from a database for a typical household throughout the year, as output. Finally, a quantitative analysis of the economic and environmental potentials of the TAHP system is conducted.

According to the HOTMAPS PROJECT [45], Finland has a relatively higher year-round heating demand compared to other European countries, making it an ideal candidate for investigating the feasibility of the proposed thermoacoustic heat pump. Fig. 10 presents the heat demand and average air-temperature data [43] of Finland over a year. The hourly heat demand ( $Q_{dem,h}$ ) can be calculated as  $Q_{dem,h} = Q_{dem,y} \times n_h \times A_d$ , where  $Q_{dem,y}$  denotes the annual total heat load demand and is taken as 169 kWh/m<sup>2</sup> here [45],  $n_h$  is the hourly heat load norm according to the HOTMAPS PROJECT [45], and  $A_d$  denotes the average floor area of occupied dwellings and is taken 97.6 m<sup>2</sup> here according to the EU Buildings Database [46]. Based on the distribution condition of hourly heat demand, we define the period of relatively greater need for heating ( $Q_{dem,h} \geq 1$  kW) as the heating demand season.

The heating performance of the TAHP system at varying heating temperatures and heat-source temperatures, obtained from the neural net-

Table 3

Economic and environmental parameters and the annual potential of the TAHP system.

Parameter	Value
Efficiency of gas boiler, $\eta_{boil}$	82% [47]
Natural gas price, $c_{ng}$	0.0563 €/kWh [47]
CO <sub>2</sub> emission factor for natural gas, $f_{ng}$	0.206 kgCO <sub>2</sub> /kWh [48]
Cost of unit CO <sub>2</sub> emission, $c_{CO2}$	0.12 €/kgCO <sub>2</sub> [49]
Annual fuel energy saving, $FES$	20.1 MWh/year
Annual total cost saving, $TCS$	1629.7 €/year
Annual environmental penalty cost saving, $EPCS$	497.2 €/year
Annual energy cost saving, $C_s$	1132.5 €/year
Annual CO <sub>2</sub> emission reduction, $ER$	4143.7 kgCO <sub>2</sub> /year

work model, is shown in Fig. 11.  $Q_{out}$  and COP of the TAHP system both rise with the increase of heating and heat-source temperatures. By taking the hourly heat demand as the output heating capacity and average air temperature as the heat-source temperature in the neural network model, the hourly heating temperature, as well as COP can be obtained, as shown in Fig. 12. On cold winter days, not only is the heat demand greater, but the temperature difference between the heat sink and heat source is also larger, requiring a relatively higher heating temperature. During the defined heating demand season, there is a visible demarcation in the variation of  $T_{dem}$ , as shown in Fig. 12 (a). The TAHP system can be considered to operate in two modes, medium temperature mode ( $T_h \geq 250$  °C) and low-temperature mode ( $T_h < 250$  °C), depending on the driven heat source grade level, i.e.: medium/low-grade heat source. The system obtains promising heating performance in both modes with a COP higher than 1.24. The COP of TAHP in mid-temperature mode is superior to that in low-temperature mode, which fluctuates relatively less.

The environmental and economic potential of the TAHP system is then investigated when it is entirely driven by waste heat without using electricity. The economic and environmental calculation models are listed in Appendix. B. Monthly total cost savings (TCS) and CO<sub>2</sub> emission reduction (ER) are estimated assuming the hourly heat demand is precisely covered, and the results are shown in Fig. 13. Table 3 lists the annual economic and environmental parameters used in the calculations and the annual potential of the TAHP system. The results show that an individual TAHP system can achieve a fuel energy saving of 20.1 MWh, a total cost saving of 1629 €, and an emission reduction of 4143 kgCO<sub>2</sub> over a year, demonstrating promising prospects for domestic heating applications in the future.

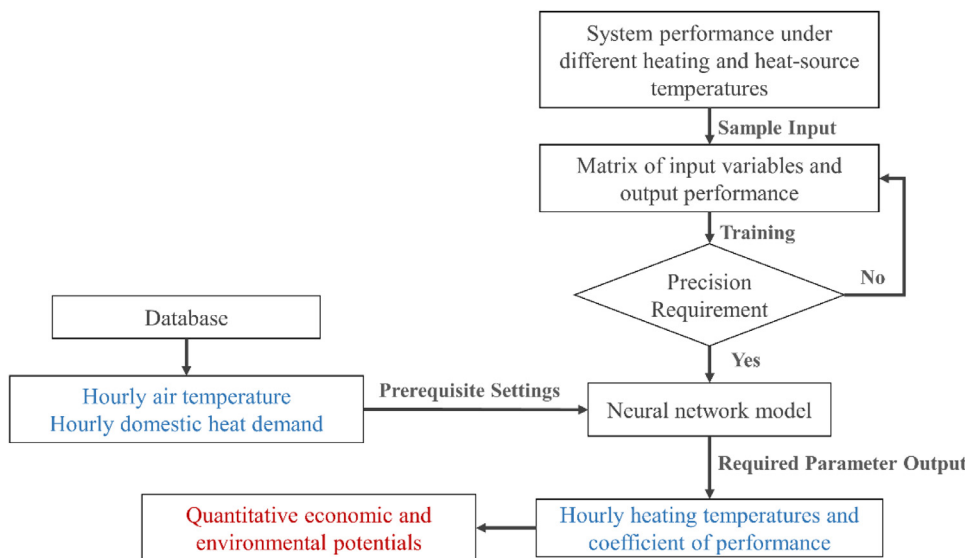


Fig. 9. The flow chart of economic and environmental analyses combining neural network model. (Prerequisite: to meet the heat demand in domestic application with output heating capacity of the TAHP system)

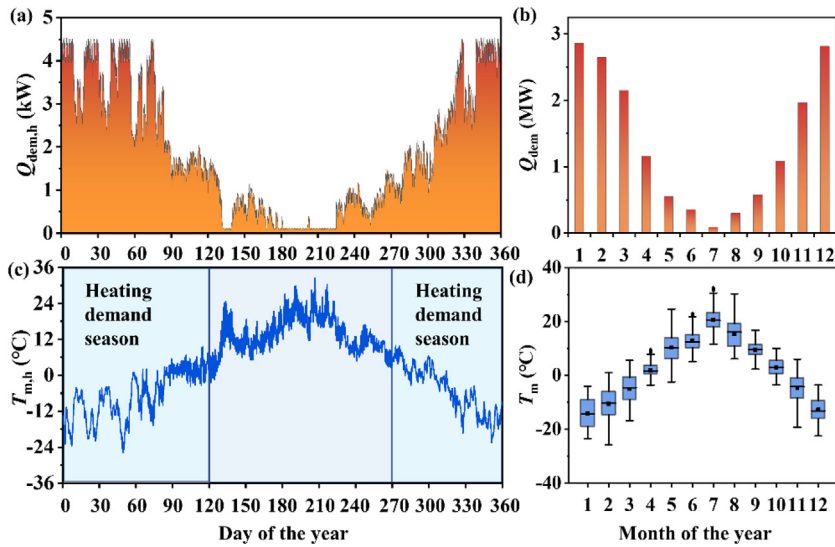


Fig. 10. (a) Hourly heat demand over a year, (b) monthly heat demand over a year, (c) hourly average air-temperature over a year, and (d) monthly air-temperature conditions over a year.

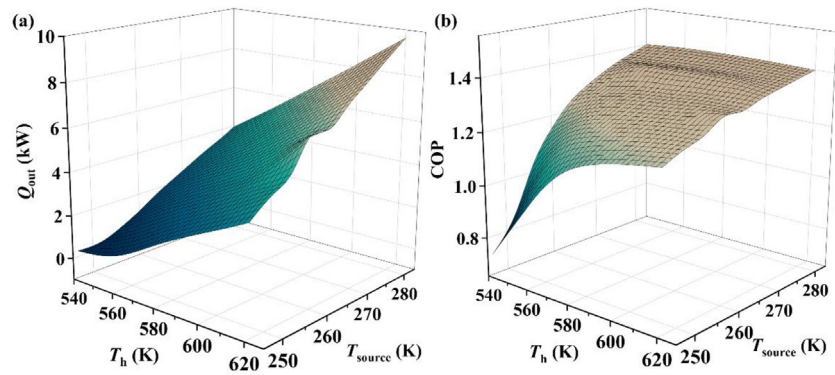


Fig. 11. Neural network model for the heating performance of thermoacoustic heat pump under different heating temperatures ( $T_h$ ) and heat-source temperatures ( $T_{source}$ ) on (a) output heating capacity ( $Q_{out}$ ) and (b) coefficient of performance (COP) ( $T_{sink}=55\text{ }^\circ\text{C}$ ).

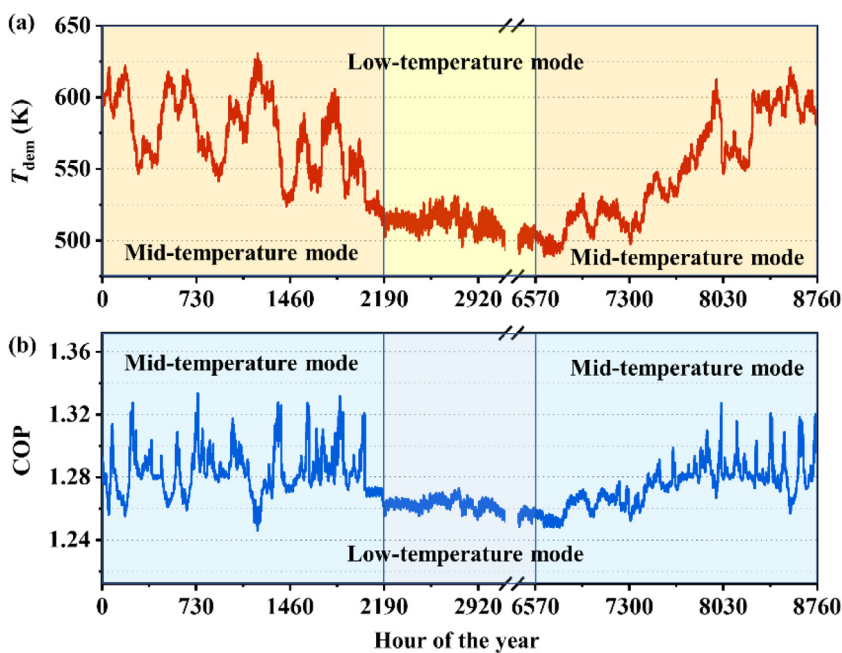


Fig. 12. Hourly heating temperature demand and coefficient of performance of the TAHP system at the heating demand season. The heat-source temperature is equal to the air-temperature and the output heating capacity is equal to the heat demand ( $T_{sink}=55\text{ }^\circ\text{C}$ ).

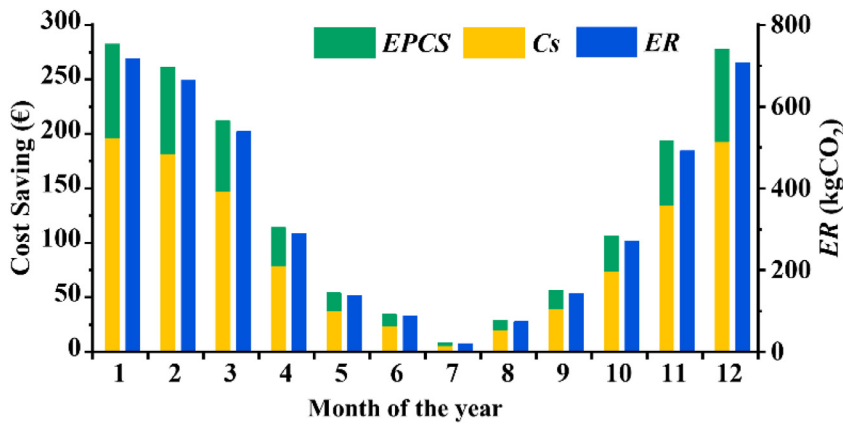


Fig. 13. Monthly total cost saving (TCS) and CO<sub>2</sub> emission reduction (ER) over a year. The TCS includes the environmental penalty cost saving (EPCS) and energy cost saving (C<sub>s</sub>).

Although thermoacoustic heat pump technology holds promise for domestic heating applications, it is still in the early stages of development. Several challenges must be overcome to realize its market potential, particularly in terms of investment costs. The core components of thermoacoustic heat pumps, such as regenerator structures requiring specific porosity wire mesh and heat exchangers made of copper, involve relatively expensive materials. To make thermoacoustic heat pumps commercially viable, cost reduction through mass production and commercialization is necessary. Another cost-related factor is the use of high-pressure helium as the working gas, which can be expensive. While nitrogen could be an alternative, it would compromise the system's performance. Therefore, there is a potential trade-off between cost and performance that needs to be considered. Addressing these cost-related issues is crucial for the successful implementation of thermoacoustic heat pumps as a renewable household heating technology and for effectively harnessing waste heat recovery.

## 6. Conclusions

This study introduces a novel heat-driven thermoacoustic heat pump (TAHP) system with a single direct-coupling configuration, which has the potential to utilize medium/low-grade heat for domestic heating. Initially, the working principle of the heat-driven TAHP system was described. Subsequently, the acoustic field characteristics of the TAHP system were investigated using numerical methods, considering various parameters such as working temperatures and pressures. A comparison was then made between the TAHP system and the absorption heat pump at different temperature lifts. Finally, the potential of the TAHP system for domestic heating was analyzed from environmental and economic perspectives.

- (1) The introduced TAHP system demonstrates satisfactory heating performance under conventional heat pump operating conditions, capable of delivering an output heating capacity ranging from 3 kW to 7 kW, with a coefficient of performance (COP) ranging from 1.28 to 1.42, when the heat-source temperature is 7 °C and the heat-sink temperature falls within the range of 50 °C to 70 °C.
- (2) In scenarios of atypical heating demand, the TAHP system exhibits promising prospects in a wide temperature lift range ( $\Delta T > 60$  °C). It has been demonstrated to function effectively even at low heat-source temperatures ( $T_{\text{source}} < 0$  °C), thereby offering a complementary solution to the existing domestic heating methods, particularly in addressing the gap in large temperature differences and low heat-source temperatures.
- (3) The utilization of the TAHP system can significantly reduce reliance on electricity. Economic and environmental analyses reveal that an individual TAHP system can yield a fuel energy saving of 20.1 MWh and reduce emissions by 4143 kgCO<sub>2</sub> over the

course of a year. When considering both the energy and environmental savings, a total cost reduction of 1629 €/year can be achieved. These findings underscore the advantages of thermoacoustic technology as a viable and environmentally-friendly alternative.

## Declaration of Competing Interest

The authors declare that they have no known competing financial interests or personal relationships that could have appeared to influence the work reported in this paper.

## CRediT authorship contribution statement

**Yiwei Hu:** Methodology, Software, Validation, Investigation, Visualization, Writing – original draft. **Kaiqi Luo:** Investigation, Writing – review & editing. **Dan Zhao:** Investigation, Writing – review & editing. **Zhanghua Wu:** Investigation, Writing – review & editing. **Yupeng Yang:** Validation, Investigation. **Ercang Luo:** Supervision, Project administration, Funding acquisition, Writing – review & editing. **Jingyuan Xu:** Conceptualization, Methodology, Formal analysis, Visualization, Supervision, Writing – review & editing.

## Acknowledgments

This research was financially supported by the [National Natural Science Foundation of China](#) (Grant No. 51876213 and No. 51976230), Strategic Priority Research Programme, CAS (No. XDA21080300), and the Open Project of CAS Laboratory of Cryogenics, No. CRYO2 02214. D. Z is financially supported by University of Canterbury with the award No. 452DISDZ.

## Appendix A

The coefficient of performance (COP) of the system can be expressed as

$$COP = \frac{Q_{out}}{Q_{e,in}} \quad (A1)$$

where

$$Q_{out} = Q_{e,out} + Q_{hp,out} \quad (A2)$$

$Q_{out}$  denotes the output heating capacity of the system,  $Q_{e,out}$  and  $Q_{hp,out}$  are the output heat from the SHX<sub>e</sub> and SHX<sub>h</sub>, respectively.  $Q_{e,in}$  is the input heat to HHX<sub>e</sub>.

Eq. (A3) gives the relative Carnot efficiency of performance of the system,

$$\eta = \frac{COP}{\frac{T_{sink}}{T_h} + \frac{T_h - T_{sink}}{T_h} \times \frac{T_{sink}}{T_{sink} - T_{source}}} \quad (A3)$$

where  $T_{sink}$  and  $T_{source}$  are the temperatures of the heat sink and heat source, respectively.

Appendix B

In addition to heating capacity and system efficiency, the fuel energy saving (FES), energy cost saving ( $C_s$ ), environmental penalty cost saving (EPCS), and potential CO<sub>2</sub> emission reduction (ER) have been explored to show the environmental and economic potentials of the system. FES is expressed as follows:

$$FES = \frac{Q_{out}}{\eta_{boi}} \times \tau_o \tag{B1}$$

where  $\eta_{boi}$  and  $\tau_o$  are the efficiency of the conventional boiler and operating time, respectively.

$$C_s = \frac{Q_{out}}{\eta_{boi}} \times c_{ng} \times \tau_o \tag{B2}$$

where  $c_{ng}$  is the of piped natural gas price.

$$ER = \frac{Q_{out}}{\eta_{boi}} \times f_{ng} \times \tau_o \tag{B3}$$

where  $f_{ng}$  is the CO<sub>2</sub> emission factor of natural gas.

$$EPCS = ER \times c_{CO_2} \tag{B4}$$

where  $c_{CO_2}$  is the cost of unit CO<sub>2</sub> emission. The total cost saving, TCS, is employed to estimate the overall economic and environmental potential, avoiding energy bill and environmental penalty cost,

$$TCS = EPCS + C_s \tag{B5}$$

Appendix C

Table C1.

Table C1

The thermodynamic parameters at the key components under specific condition ( $T_{sink} = 55\text{ }^\circ\text{C}$ ,  $T_{source} = 7\text{ }^\circ\text{C}$ ,  $T_h = 300\text{ }^\circ\text{C}$ ).

Component		SHX <sub>e</sub>	REG <sub>e</sub>	HHX <sub>e</sub>	TBT <sub>e</sub>	SHXH	REH <sub>h</sub>	HSHX <sub>h</sub>	TBT <sub>h</sub>
P  (bar)	inlet	318	318	310	310	310	309	294	289
	outlet	318	310	310	310	309	294	289	287
$\theta_p$ (°)	inlet	45.7	45.5	44.6	44.3	44.2	44.1	45.8	45.2
	outlet	45.5	44.6	44.3	44.2	44.1	45.8	45.2	44.8
U  (m <sup>3</sup> /s)	inlet	0.0174	0.017	0.022	0.022	0.024	0.024	0.023	0.023
	outlet	0.017	0.022	0.022	0.024	0.024	0.023	0.023	0.03
$\theta_U$ (°)	inlet	83.2	81.5	59.2	57.8	19.7	18.4	6.5	5.4
	outlet	81.5	59.2	57.8	19.7	18.4	6.5	5.4	-9.5
$\theta_{p-U}$ (°)	inlet	-37.5	-36	-14.7	-13.3	24.5	25.7	39.3	39.8
	outlet	-36	-14.7	-13.3	24.5	25.7	39.3	39.8	54.2
$W_a$ (kW)	inlet	2.2	2.2	3.4	3.3	3.3	3.3	2.6	2.5
	outlet	2.2	3.4	3.3	3.3	3.3	2.6	2.5	2.5
$T_s$ (°C)	inlet	331	340	562	564	332	332	378	278
	outlet	340	562	564	332	332	378	278	293

References

- [1] S. Tsemekidi Tzeiranaki, P. Bertoldi, L. Castellazzi, M. Gonzalez Torres, et al. Joint Research Centre, Energy Consumption and Energy Efficiency Trends in the EU : 2000-2020, Publications Office of the European Union, 2022.
- [2] European Environment Agency, Indicator Assessment - Data and Maps - Progress on Energy Efficiency in Europe, 2021. Available from: <https://www.eea.europa.eu/data-and-maps/indicators/progress-on-energy-efficiency-in-europe-3/assessment>.
- [3] M. Papapetrou, G. Kosmadakis, A. Cipollina, U. La Commare, G. Micale, Industrial waste heat: Estimation of the technically available resource in the EU per industrial sector, temperature level and country, Appl. Therm. Eng. 138 (2018) 207–216.
- [4] I. Johnson, W.T. Choate, A. Davidson, Waste Heat Recovery, Technology and Opportunities in U.S. Industry, United States, 2008.
- [5] L.W. Yang, R.J. Xu, N. Hua, Y. Xia, W.B. Zhou, T. Yang, et al., Review of the advances in solar-assisted air source heat pumps for the domestic sector, Energy Convers. Manag. 247 (2021) 114710.
- [6] A.V. Olympios, P. Sapin, J. Freeman, C. Olkis, C.N. Markides, Operational optimization of an air-source heat pump system with thermal energy storage for domestic applications, Energy Convers. Manag. 273 (2022) 116426.
- [7] J. Love, A.Z.P. Smith, S. Watson, E. Oikonomou, A. Summerfield, C. Gleeson, et al., The addition of heat pump electricity load profiles to GB electricity demand: Evidence from a heat pump field trial, Appl. Energy 204 (2017) 332–342.
- [8] Y. Yang, J. Chi, Z. Wu, R. Yang, J. Xu, L. Zhang, et al., A heat-driven combined cooling and heating system based on thermoacoustic technology, Appl. Phys. Lett. 120 (2022) 23902 -.
- [9] G. Chen, L. Tang, B. Mace, Z. Yu, Multi-physics coupling in thermoacoustic devices: a review, Renew. Sustain. Energy Rev. 146 (2021) 111170.
- [10] D. Haywood, Investigation of Stirling-Type Heat-Pump and Refrigerator Systems Using Air as the Refrigerant, New Zealand: University of Canterbury, 2004.
- [11] M.M. Bassem, Y. Ueda, A. Akisawa, Thermoacoustic Stirling Heat Pump Working as a Heater, Appl. Phys. Express 4 (2011) 107301.
- [12] Z. Yang, C. Yanyan, Y. Guoyao, L. Ercang, Z. Yuan, Experimental investigation on a linear-compressor driven travelling-wave thermoacoustic heat pump, Energy Procedia 75 (2015) 1844–1849.
- [13] L. Ke, Y. Guoyao, Z.J. Yibing, Theoretical and experimental study of free piston Stirling heat pump. 36 (2015) 41–5.
- [14] A. Widyaparaga, T. Hiromatsu, Deendarlianto, M. Kohno, Y. Takata, Acoustic field alteration in a 100 Hz dual acoustic driver straight tube travelling wave thermoacoustic heat pump for thermoacoustic heat transport control, Int. J. Heat Mass Transf. 151 (2020) 119274.
- [15] M.H. Ahmadi, M.A. Ahmadi, A.H. Mohammadi, M. Mehrpooya, M. Feidt, Thermodynamic optimization of Stirling heat pump based on multiple criteria, Energy Convers. Manag. 80 (2014) 319–328.
- [16] M.H. Ahmadi, M.A. Ahmadi, R. Bayat, M. Ashouri, M. Feidt, Thermo-economic optimization of Stirling heat pump by using non-dominated sorting genetic algorithm, Energy Convers. Manag. 91 (2015) 315–322.
- [17] I. Barreno, S.C. Costa, M. Cordon, I. Urrutibea, X. Gomez, M. Mateos, Dynamics of an oscillating Stirling heat pump, Appl. Energy 136 (2014) 704–711.

- [18] Y. Sun, J. Hu, E. Luo, L. Zhang, K. Luo, Z. Wu, A gas-fired heat-driven thermoacoustic heat pump for winter heating, in: Proceedings of the 25th IIR International Congress of Refrigeration in Montreal, Canada, 2019.
- [19] U. Khan, R. Zevenhoven, T.M. Tveit, Evaluation of the environmental sustainability of a Stirling cycle-based heat pump using LCA, *Energies* 13 (2020) 4469.
- [20] C.H. Cheng, H.S. Yang, H.X. Chen, Development of a beta-type Stirling heat pump with rhombic drive mechanism by a modified non-ideal adiabatic model, *Int. J. Energy Res.* 44 (2020) 5197–5208.
- [21] J. Xu, E. Luo, S. Hochgreb, A thermoacoustic combined cooling, heating, and power (CCHP) system for waste heat and LNG cold energy recovery, *Energy* 227 (2021) 120341.
- [22] R. Yang, N. Blanc, G.Z. Ramon, Theoretical performance characteristics of a travelling-wave phase-change thermoacoustic heat pump, *Energy Convers. Manag.* 254 (2022) 115202.
- [23] G. Chen, L. Tang, Z. Yu, Modeling and analysis of a dual-acoustic-driver thermoacoustic heat pump, *Therm. Sci. Eng. Prog.* 30 (2022) 101270.
- [24] K. De Blok, Low operating temperature integral thermo acoustic devices for solar cooling and waste heat recovery, *J. Acoust. Soc. Am.* 123 (2008) 3541.
- [25] H. Wang, L. Zhang, G. Yu, J. Hu, E. Luo, Y. Ma, et al., A looped heat-driven thermoacoustic refrigeration system with direct-coupling configuration for room temperature cooling, *Sci. Bull.* 64 (2019) 8–10.
- [26] T. Bi, Z. Wu, W. Chen, L. Zhang, E. Luo, B. Zhang, Numerical and experimental research on a high-power 4-stage looped travelling-wave thermoacoustic electric generator, *Energy* 239 (2022) 122131.
- [27] Z. Wu, G. Yu, L. Zhang, W. Dai, E. Luo, Development of a 3kW double-acting thermoacoustic Stirling electric generator, *Appl. Energy* 136 (2014) 866–872.
- [28] X. Wang, Z. Wu, L. Zhang, J. Hu, E. Luo, Traveling-wave thermoacoustic refrigerator for room temperature application, *Int. J. Refrig.* 120 (2020) 90–96.
- [29] D. Gedeon, Sage - object-oriented software for cryocooler design, in: Proceedings of the 8th International Cryocooler Conference (Cryocoolers 8), Vail, Colorado, 1994, pp. 281–292.
- [30] J. Chi, Y. Yang, Z. Wu, R. Yang, P. Li, J. Xu, et al., Numerical and experimental investigation on a novel heat-driven thermoacoustic refrigerator for room-temperature cooling, *Appl. Therm. Eng.* 218 (2023) 119330.
- [31] X. Wang, J. Xu, Z. Wu, E. Luo, A thermoacoustic refrigerator with multiple-bypass expansion cooling configuration for natural gas liquefaction, *Appl. Energy* 313 (2022) 118780.
- [32] J. Xu, J. Hu, E. Luo, L. Zhang, W. Dai, A cascade-looped thermoacoustic driven cryocooler with different-diameter resonance tubes. Part I: Theoretical analysis of thermodynamic performance and characteristics, *Energy* 181 (2019) 943–953.
- [33] J. Xu, J. Hu, Y. Sun, H. Wang, Z. Wu, J. Hu, et al., A cascade-looped thermoacoustic driven cryocooler with different-diameter resonance tubes. Part II: Experimental study and comparison, *Energy*. 207 (2020) 118232.
- [34] Y. Hu, X. Wang, Z. Wu, L. Zhang, G. Chen, J. Xu, et al., A thermoacoustic cooler with a bypass expansion for distributed-temperature heat loads, *Appl. Phys. Lett.* 121 (2022) 203905.
- [35] E. Van Kenhove, P. De Vlieger, J. Laverge, A. Janssens, Towards energy efficient and healthy buildings: trade-off between Legionella pneumophila infection risk and energy efficiency of domestic hot water systems, in: Proceedings of the 12th REHVA World Congress, 2016.
- [36] Air Conditioners, Liquid Chilling Packages and Heat Pumps For Space Heating and Cooling And Process Chillers, with Electrically Driven Compressors, BSI, 2018.
- [37] L. Guo, D. Zhao, S. Becker, Temperature difference and stack plate spacing effects on thermodynamic performances of standing-wave thermoacoustic engines driven by cryogenic liquids and waste heat, *J. Therm. Sci.* 31 (2022) 1434–1451.
- [38] L. Guo, D. Zhao, J. Xu, M.O. Tokhi, H.R. Karimi, Predicting unsteady heat-fluid interaction features and nonlinear acoustic behaviors in standing-wave thermoacoustic engines using unsteady RANS, LES and hybrid URANS/LES methods, *Int. Commun. Heat Mass Transf.* 142 (2023) 106617.
- [39] Y. Hu, J. Xu, K. Luo, G. Chen, L. Zhang, Z. Wu, et al., A heat-driven thermoacoustic heat pump with a single direct-coupling configuration capable of utilizing medium/low-grade heat for domestic applications, in: Proceedings of the 14th International Conference on Applied Energy, Bochum, Germany, 2022.
- [40] R. Wang, J. Hu, Z. Jia, L. Zhang, E. Luo, Study on the temperature adaptability of free-piston Stirling heat pump, *Energy Convers. Manag.* 249 (2021) 114864.
- [41] Y. Li, L. Fu, S. Zhang, X. Zhao, A new type of district heating system based on distributed absorption heat pumps, *Energy* 36 (2011) 4570–4576.
- [42] Y. Li, L. Wang, M. Zhu, W. Wang, Optimization study of distillation column based on Type I absorption heat pump, *Appl. Therm. Eng.* 116 (2017) 33–42.
- [43] Y. Li, Y. Ding, M. Cao, Optimization of energy-saving distillation system of absorption heat pump based on intermediate heat exchange, *Appl. Therm. Eng.* 213 (2022) 118721.
- [44] J. Fu, R. Yang, X. Li, X. Sun, Y. Li, Z. Liu, et al., Application of artificial neural network to forecast engine performance and emissions of a spark ignition engine, *Appl. Therm. Eng.* 201 (2022) 117749.
- [45] S. Pezzutto, S. Zambotti, S. Croce, P. Zambelli, G. Garegnani, C. Scaramuzzino, R.P. Pascuas, A. Zubaryeva, F. Haas, D. Exner (EURAC), Andreas Müller (e-think), Michael Hartner (TUW), Tobias Fleiter, Anna-Lena Klingler, Matthias Kühnbach, Pia Manz, Simon Marwitz, Matthias Rehfeldt, Jan Steinbach, Eftim Popovski (Fraunhofer ISI) Reviewed by Lukas Kranzl, Sara Fritz (TUW) Hotmaps Project, D2.3 WP2 Repor – Open Data Set for the EU28, 2018. Available from: [www.hotmaps-project.eu](http://www.hotmaps-project.eu) [accessed 17/03/2023].
- [46] EU Buildings Database | Energy (europa.eu). Available from: <https://ec.europa.eu/energy> [accessed 17/03/2023].
- [47] K. Wang, M. Herrando, A.M. Pantaleo, C.N. Markides, Technoeconomic assessments of hybrid photovoltaic-thermal vs. conventional solar-energy systems: case studies in heat and power provision to sports centres, *Appl. Energy* 254 (2019) 113657.
- [48] Emission Factor Database. Available from: <https://www.eea.europa.eu/publications/emep-eea-guidebook-2019/emission-factors-database> [accessed 17/03/2023].
- [49] B. Carlsson, M. Meir, J. Rekstad, D. Preiß, T. Ramschak, Replacing traditional materials with polymeric materials in solar thermosiphon systems – Case study on pros and cons based on a total cost accounting approach, *Sol. Energy* 125 (2016) 294–306.